Hindawi
Advances in Materials Science and Engineering
Volume 2023, Article ID 5264233, 13 pages
https://doi.org/10.1155/2023/5264233

Research Article

Experimental and Numerical Investigation of Integrated Steel Shear Walls with Varying Web Width-to-Thickness Ratios

Doo-Yong Lee, Bong-Ho Cho, and Dam-I. Jung

Department of Architectural Engineering, Ajou University, 206 World cup-ro, Yeongtong-gu, Suwon-si, Gyeonggi-do 16499, Republic of Korea

Correspondence should be addressed to Bong-Ho Cho; bhcho@ajou.ac.kr

Received 18 January 2023; Revised 11 April 2023; Accepted 24 April 2023; Published 9 May 2023

Academic Editor: Ivan Giorgio

The cold-formed steel-framed shear wall sheathed with steel sheet is widely used as a lateral force-resisting system for light-framed construction. However, the boundary conditions of the screw joint are not clear when steel is screwed to the frame. To address this issue, experimental methods have been used to calculate shear strength, but these methods have many limiting factors. In this study, we investigate the structural performance of integrated steel shear walls with varying web width-to-thickness ratios as an alternative to steel-sheathed shear walls used in light-gauge steel frames. The proposed design equation for cold-formed steel integrated shear walls is validated by three specimens and 72 finite element models. This equation allows designers to determine the strength of integrated steel shear walls without conducting full-scale shear-wall tests.

1. Introduction

Light-gauge steel frames are built using cold-formed steel (CFS) members. These members are lightweight and, thus, exhibit good seismic properties (Chini and Gupta [1]; Yong et al. [2]; and Yang and Yang [3]). Unlike load-bearing walls (resisting both vertical and lateral loads, simultaneously) applied to general structures, lightweight steel structures use shear walls, which resist only lateral loads. In a lightweight steel structure, the wall is composed of a track (horizontal member) and stud (horizontal member), as shown in Figure 1(a). The stud and track of the thin plate are pin-connected with screws; hence, if there is no shear wall, the structure becomes unstable when a horizontal load is applied. Lateral force-resisting systems in light-gauge steel-frame constructions commonly employ CFS-framed shear walls sheathed with thin-walled steel sheets. The sheathing is fastened to the frame around the boundary elements and in the inner stud using self-drilling self-tapping screws.

The nominal shear strength of the hot-rolled steel plate welded to the frame can be calculated using the engineering theoretical formula considering the strength of the tensile field that acts after shear buckling occurs. However, for the cold-formed steel-framed shear wall sheathed with steel screwed to the frame in light-gauge steel frames, the design method that experimentally calculates the shear strength is adopted because the boundary conditions of the screw joint are not clear.

AISI S240-15 adopts a definition of the nominal strength of cold-formed steel-sheathed shear walls based on experimental results, not engineering theory. According to AISI S240-15, the first method for calculating the nominal shear strength of a steel-sheathed shear wall was proposed by Serrette [5] based on experimental results. In this method, the unit nominal shear strength is provided in a table when the thickness of the steel plate is 0.46 mm, 0.68 mm, 0.76 mm, and 0.84 mm and the screw spacing is 150 mm, 100 mm, 75 mm, and 50 mm in the steel plate shear wall, and it is calculated by multiplying the nominal shear strength by the length of the shear wall. Since the nominal shear strength of steel-sheathed shear walls is defined based on Serrette's experimental findings [5]rather than a closed-form equation, there are numerical limitations on the steel plate thickness and screw spacing.

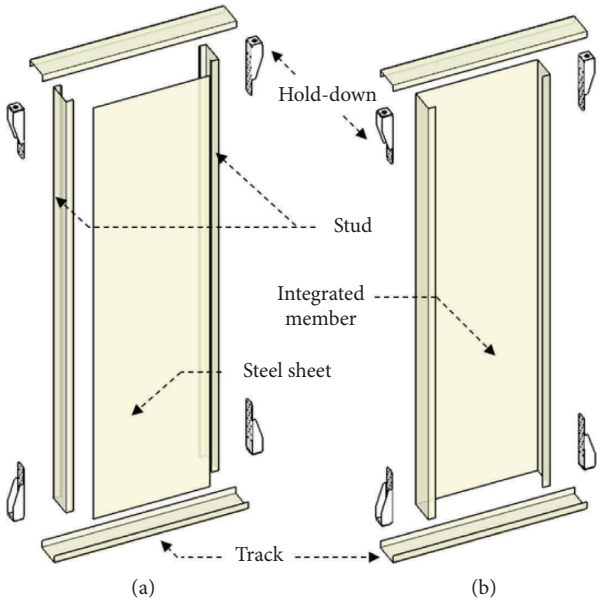

Figure 1: Components of a (a) steel-sheathed shear wall and (b) integrated steel shear wall (Lee et al. [4]).

The second method for calculating the nominal shear strength of a steel-sheathed shear wall is the effective strip method proposed by Yanagi and Yu [6]. The effective strip method added to AISI S240-15 defines the nominal shear strength as a small value by comparing the nominal shear strength of the joint strength between the screw and steel plate of the steel-plate shear wall with that of the tensile yielding of the strip in the steel plate. This method also has restrictions on the thickness of the cold-forming steel member (0.838–1.37 mm), the thickness of the steel sheet (0.457–0.838 mm), screw spacing (50.8–152 mm), and the aspect ratio of the steel sheet (height/width = 1–4). However, this method has fewer strict limitations than that for calculating the nominal shear strength of a steel-sheathed shear wall based on the experimental basis of Serrette [5]. According to Yu [7, 8] and Wang et al. [9], steel-sheathed shear walls mainly exhibit failure modes, such as sheathing buckling and screw connection failure. To be sufficiently exhibited, the strength of the screw joint must be sufficient; however, in this case, the required number of screws increases.

Several alternatives have been proposed to enhance the structural performance of steel-sheathed shear walls [Hong et al. [10]; Fiorino et al. [11]; Zhang et al. [12]; Zhang et al. [13]; and Rahimibala et al. [14]). In this study, we conducted research on a new type of shear wall called the integrated steel shear wall, which can be applied to lightweight steel structures, as introduced in Lee et al.'s study [4]. In integrated steel shear walls, the steel plate and stud of the steel-plate shear wall are replaced with a rib C-shaped steel member (integrated member), as shown in Figure 1(b). The screw joint between the steel plate and stud of the steel-plate shear wall is omitted from the integral steel-plate shear wall. Hence, from the viewpoint of the effective strip method, which can be used to calculate the nominal shear strength of a steel plate shear wall, an integrated steel shear wall is expected to improve the joint strength and increase the shear strength more than a steel-sheathed shear wall. Additionally, the use of integrated steel shear walls can improve constructability.

The integral member is a rib C-shaped steel with a large web width-to-thickness ratio. The web width-to-thickness ratio of the effective-width method and direct-strength method (applicable when calculating the nominal bending strength considering local buckling specified in AISI S100-16 [15]) should be 200 and 300 or less, respectively, and the ideal maximum width of a one-piece member is 640 mm (finishing material production standard 600 mm + cross section width 40 mm according to the product standard of studs, and the maximum distance between studs is 610 mm). Because the web width-to-thickness ratio of the member is 640 when the web thickness is 1 mm, the AISI S100-16 standard [15] cannot be applied. Therefore, as a follow-up to Lee et al.'s study [4], the aim of this study is to develop and verify a design formula for the nominal shear strength of the integrated steel shear wall as an alternative to the steel-sheathed wall used in light-gauge steel frames. While Lee et al. [4] focused on the structural performance of the integrated steel shear wall with stud reinforcement, this study investigates the structural performance of the integrated steel shear wall with an integrated member that has varying web widths.

2. Estimated Strength of the Integrated Steel Shear Wall According to AISI S100-16

As previously explained, the strength of an integrated steel shear wall cannot be estimated because of the limits in AISI S100-16 [15] for the width-to-thickness ratio of the web. In this section, we intend to investigate the predicted strength of the integral steel sheet shear wall when AISI S100-16 is applied without considering limit values such as the web width-to-thickness ratio.

2.1. The Estimated Shear Strength, V_{ESB}, Governed by Elastic Shear Buckling. The nominal shear strength of the cold-formed rib C-beams is determined by the strength when shear buckling dominates in AISI S100-16. The predicted shear strength of the integral steel sheet shear wall against shear buckling was considered when the member's yield, inelastic buckling, and elastic buckling dominated. Because the width-to-thickness ratio of the integrated steel shear wall exceeds the AISI S100-16 standard ($1.227 > \lambda_v$), the shear strength (V_{ESB}) of the integrated steel shear wall dominated by elastic shear buckling is given by the following equation:

$$\text{For } 1.227 > \lambda_v, V_{ESB} = V_{cr} = A_w F_{cr} = \frac{0.904 E k_v t^3}{w}. \quad (1)$$

2.2. The Estimated Shear Strength, V_{ESM}, According to the Effective Strip Method. Yanagi and Yu [6] proposed an effective strip method for estimating the nominal shear

strength of a steel-sheathed shear wall based on a strip model. The most important difference between hot-rolled steel sheet shear walls and cold-formed steel sheet shear walls is the sheet's boundary condition. In a cold-formed steel sheet shear wall screwed to a boundary element other than a weld joint, damage to the screw (such as pull-out, pull-over, and net section failure) and tearing of the steel sheet may occur. The shear strength of the shear wall is controlled by the tensile strength of the effective sheathing strip, which is determined as the lesser of the fasteners' tensile strength and the yield strength of the effective sheathing strip. Effective strip width is determined by considering factors such as the aspect ratio of the steel plate, the member size of the boundary element, the screw connection between the steel plate and the boundary element of the steel plate, and the material properties of the steel-plate shear-wall component. However, for an integrated steel shear wall, because there is no stud-steel plate screw connection in the steel plate shear wall, the predicted shear strength of the integrated steel shear wall can be defined. Equation (2) shows the predicted shear strength (V_{ESM}) of the integrated steel shear wall using the tensile field defined by the effective strip method.

$$V_{\mathrm{ESM}} = 1.33 w_e t F_y \cos\alpha = 1.33\left(\rho \frac{w}{\sin\alpha}\right) t F_y \cos\alpha, \tag{2}$$

$$\rho = \frac{\left[1 - 0.55\left(\lambda - 0.08\right)^{0.12}\right]}{\lambda^{0.12}}. \tag{3}$$

To apply equation (2) to the integral steel sheet shear wall, among the factors defining ρ and $\lambda\,(= 1.736\alpha_1\alpha_2/\beta_1\beta_2\beta_3^2 a)$, the limit values of a (= 1–4), which is the aspect ratio of the steel sheet, and β_1 (= 0.457–0.838mm), which is the thickness of the steel sheet, and β_2 (= 0.838–1.37mm), which is the thickness of the steel sheet shear wall boundary element, were ignored. For screw spacing, β_3 (= 50.8–152mm), the minimum value of 50.8 mm, was considered.

2.3. The Estimated Shear Strength, V_{EWM}, by the Effective Width Method. The nominal bending strength (M_n) of a single member, such as an integrated member, is determined as the smallest value among the three values: nominal flexural strength due to member yield and lateral buckling (M_{ne}), nominal flexural strength by local buckling calculated using the effective width method (M_{nl}), and nominal flexural strength due to distortional buckling (M_{nd}). Therefore, the shear strength (V_{EWM}) according to the effective width method for bending the integrated member is the same as shown below:

$$V_{\mathrm{EWM}} = \frac{M_n}{h_1} = \frac{\min\left(M_{\mathrm{ne}}, M_{\mathrm{nl}}, M_{\mathrm{nd}}\right)}{h_1}, \tag{4}$$

where h_1 is half the height of the integrated member, except for hold-down.

3. Experiment Test

3.1. Test Protocol. To verify the structural performance of the integrated steel shear wall, three specimens with the web width (web slenderness (height-to-thickness) ratio) of the integrated member as a variable were manufactured; to contrast with the test results of the integrated steel shear wall, one shear wall sheathed with a steel sheet sheathing specimen was manufactured. Figure 2(a) displays the cross sections of the specimens, and Figures 2(d) and 2(e) show the details of the screw joint. Here, the ISW-640-1.6 and SSW-640-1.6 specimens are the same as the IP and SSP specimens in Lee et al. [4], respectively.

In the integrated steel shear wall (ISW) specimen, the track member and web of the integrated member were joined using #10 screws ($\phi = 5.2$ mm) spaced at 75 mm intervals, as shown in Figure 2(b). Additionally, the track member and lip of the integrated member were also joined at each corner using a single #10 screw. The specimens were fabricated so that the shear walls could be installed in the light-gauge steel frame. The ISW specimens consisted of an integrated member, four hold-downs, track members, and reinforced studs. The specifications of the ISW specimens were identical except for the integrated member, as illustrated in Figure 2(a). In light-gauge steel frames, studs are installed at intervals of 300 mm, 450 mm, or 600 mm according to the production standards of finishing materials (such as gypsum board and oriented strand board (OSB)) attached to the frame, and the height of the wall is generally 2,440 mm [16–18]. This was reflected in the specifications of the specimens. For the steel-sheathed shear wall (SSW) specimen, a 2440 mm high × 640 mm wide × 1.6 mm thick steel sheet was attached to the stud and track member with a single row of #10 screws spaced at intervals of 150 mm and 75 mm, respectively, as shown in Figure 2(c).

Moghimi and Ronagh [19] reported improvements in the racking resistance of shear walls and distortional buckling resistance of studs and chord members through cladding with gypsum boards. Furthermore, the AISI lateral design standard recommends a 30% increase in shear strength when using wooden sheathing (or OSB) on one side and a fully blocked gypsum board on the other side of walls subjected to wind and other types of in-plane loading. Therefore, dissimilar sheathing attached to the panel (e.g., OSB on the exterior face and gypsum board on the interior face) was ignored in this study.

For the cyclic loading tests, a 200 kN actuator (maximum stroke = ±200 mm) was attached to the left end of the spread beam (C-180 × 150 × 9.0), and lateral supports were installed at two points on the loading jig, as shown in Figure 3. To fix the specimens and apply a loading force, the spread beams were joined to the hold-down of the panel with anchor bolts and were installed above and below the panel. Because the rigidity of the floor or roof elements in the light-gauge steel frames is considerably higher than that of the shear panel, the spread beam is constrained by two columns (B-150 × 150 × 4.5) with two hinged ends on the left and right

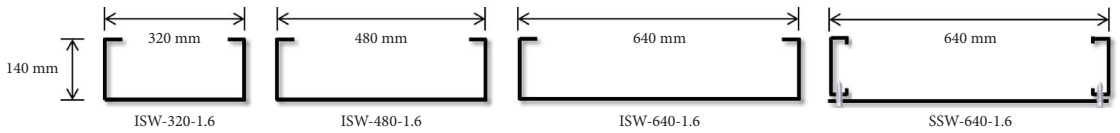

(a)

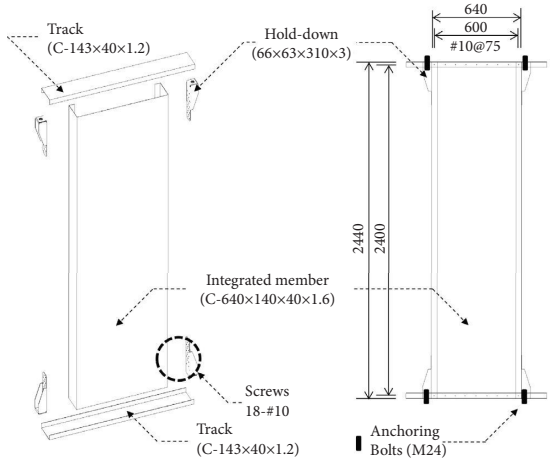

(b)

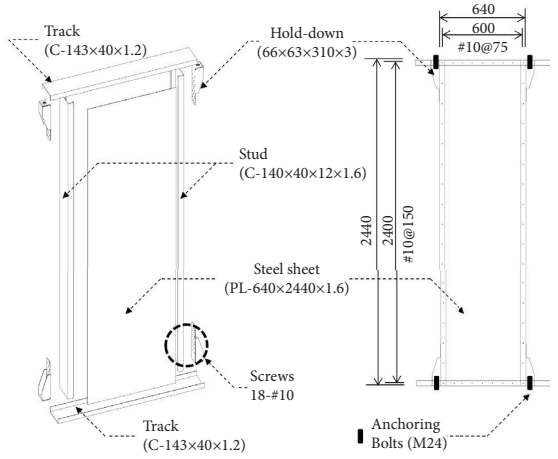

(c)

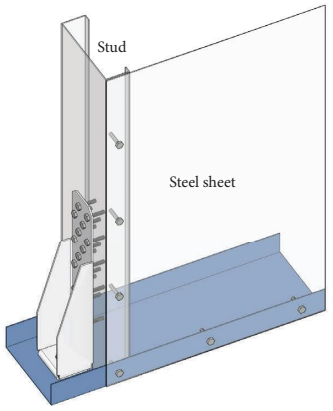

(d)

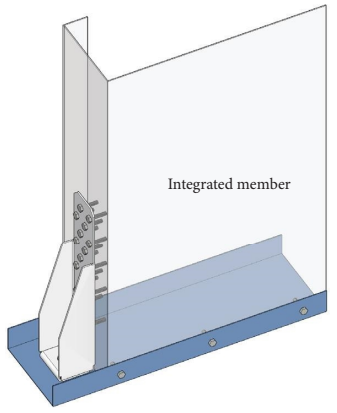

(e)

Figure 2: Configurations and details of the test specimens: (a) cross sections of the specimens, (b) ISW-640-1.6 specimen (Lee et al. [4]), (c) SSW-640-1.6 specimen (Lee et al. [4]), (d) lower left side of the SSW specimen (Lee et al. [4]), and (e) lower left side of the ISW specimens (Lee et al. [4]).

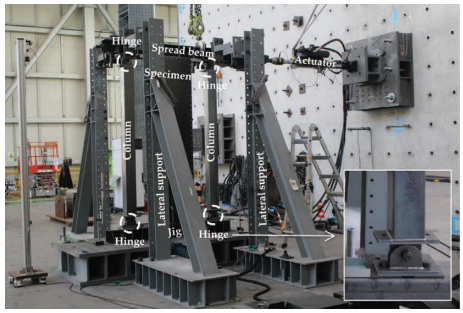

Figure 3: Test setup (Lee et al. [4]).

sides of the specimens to match the displacement in the gravity direction of the spread beam. The testing rig was designed based on studies conducted by Zeynalian and Ronagh [20] and Mirzaei et al. [21] to behave similarly to the panels in light-gauge steel frames.

The loading cycles were repeated six times for lateral drift ratios of ±0.375%, ±0.5%, and ±0.75%; four times for a lateral drift ratio of ±1.0%; and twice for lateral drift ratios of ±1.5%, ±2.0%, ±3.0%, ±4.0%, ±5.0%, ±6.0%, and ±7.0%. In this setup, a lateral drift ratio of 1.0% corresponds to a displacement of 24.4 mm. This loading protocol was adopted from the SAC protocol [22].

One horizontal and two vertical linear variable differential transducers (LVDTs) were installed. The horizontal LVDT was installed at the end of the spread beam that is not connected to the actuator, while the vertical LVDTs were mounted at the end of the spread beam to measure its rotation angle.

3.2. Material Properties. Table 1 summarizes the yield and tensile strengths of the specimen components obtained from the three coupon tensile tests.

3.3. Test Results. Figures 4 and 5 illustrate the lateral load-drift ratio relationships and failure modes of the specimens, respectively. The energy equivalent elastic-plastic (EEEP) curves for the specimens are shown in Figure 4. The key parameters (yield strength V_y, yield displacement Δ_y, and ultimate displacement Δ_u) of the EEEP curves were defined in accordance with the American Society for Testing and Materials (ASTM) E2126-19 [23].

All the ISW specimens exhibited local buckling at the bottom of the integrated member when subjected to a loading force, as shown in Figure 5. The failure of the specimen was concentrated at the bottom of the integrated member because the spread beam rotated in the in-plane direction of the specimen. For the ISW specimens, the stiffness decreased after local buckling owing to bending, whereas the strength increased. Ultimately, we found that local buckling on the upper part of the specimen due to the internal force of the tensile field dominated the maximum strength of the specimen. Regarding the ISW specimens, no failures were observed in the screws. On the other hand, for the SSW specimen, screw pull-out failure was observed at a drift ratio of 4.0%, which resulted in a significant decrease in the load-carrying capacity.

Table 2 compares the experimental and estimated shear strengths (refer to Section 2) of the specimens. During the experiment carried out in the forward direction, an out-of-plane displacement occurred, resulting in an inaccurate measurement value. Therefore, the measurement data were compared with the analysis results based on the negative directional data. Considering the estimated shear strength V_{ESB} governed by elastic shear buckling, the V_{peak}/V_{ESB} value of the ISW-320-1.6 specimen was 1.16. However, as the web width of the ISW specimen increased, the accuracy decreased significantly. According to the effective strip method, the estimated shear strength V_{ESM} accurately predicted the maximum strength V_{peak} of ISW-320-1.6 with the lowest width-to-thickness ratio among the ISW specimens, similar to the predicted shear strength V_{ESB} governed by elastic shear buckling. However, as the web width of the ISW specimen increased, the accuracy decreased significantly. The V_{peak}/V_{EWM} value of the SSW-640-1.6 specimen, which is a steel-plate shear wall, was 1.09, indicating that the value was accurately estimated even though the thickness of the steel plate (1.6 mm) exceeded the limit value (0.457–0.838 mm). V_{peak}/V_{EWM} was found to be 0.64–0.71 in the ISW specimens. In Figure 4, the strength at point A, where there was local buckling in the ISW specimen, was approximately half the shear strength V_{EWM} estimated by the nominal bending strength when bending was dominant. This is believed to be because local buckling occurred before the inaccuracy of the design formula (equation (3)), and the bending stress was illustrated by the exceeding of the dimensional limit of the web width ratio of the specimens. A comparison of the integrated steel plate shear wall specimens (ISW-320-1.6, ISW-480-1.6, and ISW-640-1.6) indicated that the greater the web width-to-thickness ratio of the integral member, the greater the maximum strength V_{peak}.

4. Finite Element Analysis

4.1. Finite Element Analysis Model. CFS finite element models were created in ABAQUS/CAE (ABAQUS, 2018) for the full-scale experiments presented in Section 3. The dimensions and thicknesses of the models were the same as those of the specimens. Kim and Lee [24] demonstrated that using a thin, shear-flexible, and isoparametric shell element of S4R5, S4R, and STRI35 is adequate for modeling steel frames. Therefore, we used the S4R5 thin-shell elements in the FEM. The finite element mesh size used in the model was approximately 5 mm × 5 mm. The closer the mesh size approaches zero, the more accurate the finite element analysis results; however, the analysis consumes a long time. Considering the mesh size as variable (2.5 mm × 2.5 mm to 20 mm × 20 mm), 5 mm × 5 mm was selected considering the analysis results and the time required for the analysis.

The effect of an initial geometric imperfection is not significantly sensitive within the elastic-buckling region of C-section cold-formed steel (Susila and Tan [25] and Craveiro et al. [26]). In this study, geometrical imperfections were not considered because the purpose of the analysis was

Table 1: The yield and tensile strengths of the CFS components of the specimens (Lee et al. [4]).

Steel	Number of coupon tests	Thickness (mm)	Maximum yield/tensile strengths (MPa)	Minimum yield/tensile strengths (MPa)	Average yield/tensile strengths (MPa)
Track	3	1.2	324.4/352.6	323.6/352.3	323.9/352.4
Integrated member, steel sheet, and stud	3	1.6	324.6/375.0	323.1/374.9	324.0/374.9

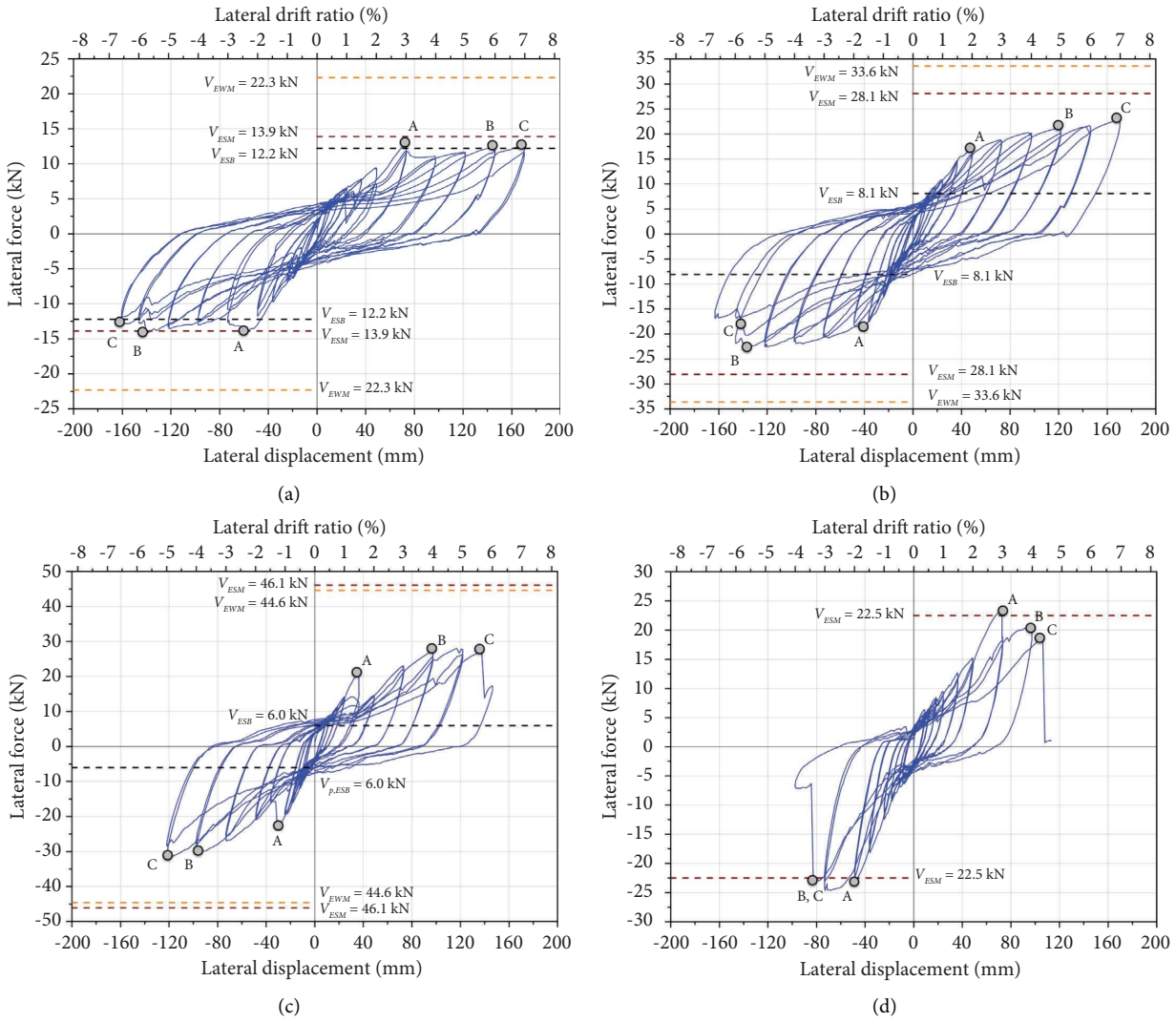

Figure 4: Lateral load-drift ratio relationships of the specimens (point A: local buckling occurred, point B: tearing occurred, and point C: maximum displacement defined by ASTM E2126-16. (a) ISW-320-1.6, (b) ISW-480-1.6, (c) ISW-640-1.6 (Lee et al. [4]), and (d) SSW-640-1.6 (Lee et al. [4]).

(a) (b) (c) (d)

Figure 5: Deformation shape of the specimens at a drift ratio of 4.0%. (a) ISW-320-1.6; (b) ISW-480-1.6; (c) ISW-640-1.6; (d) SSW-640-1.6.

Table 2: Comparison of the experimental shear strength and predicted shear strength of the specimens.

Specimens		Test results	Prediction			Comparison*		
		V_{peak} (kN)	V_{ESB} (kN)	V_{ESM} (kN)	V_{EWM} (kN)	V_{peak}/V_{ESB}	V_{peak}/V_{ESM}	V_{peak}/V_{EWM}
ISW-320-1.6	+	12.9	12.2	13.9	22.3	1.16	1.02	0.64
	−	14.2						
ISW-480-1.6	+	22.9	8.1	28.1	33.6	2.80	0.81	0.68
	−	22.7						
ISW-640-1.6**	+	28.1	6.0	46.1	44.6	5.30	0.69	0.71
	−	31.8						
SSW-640-1.6**	+	23.5	—	22.5	—	—	1.09	—
	−	24.6						

*The ultimate strength (V_{peak}) was measured in the negative direction. **See Lee et al. [4].

to predict the strengths V_{LB} when local buckling occurs for the practical use of the integrated steel shear wall.

The boundary conditions were as follows: the screw and bolt joints were tied to each other using the tie constraint (the elastic stiffness may be partially overestimated, but for ease of analysis); the reference point located at the top and bottom of the integrated member was constrained to be similar to the experimental conditions.

The failure mode of the specimens occurred at the lower part of the shear wall because of the rotation angle in the loading direction of the specimen loading beam. To match the experimental environment and constraint conditions of the analytical model, the rotation angle of the spread beam measured experimentally was also considered in the analysis.

Material nonlinearity was included in the FEM by specifying the true stress and true strain. The plasticity of the material was simulated using a mathematical model known as the incremental plasticity model, and the true stress (σ_{true}) and true plastic strain (ε_{true}) were calculated as

$$\sigma_{true} = \sigma(1 + \varepsilon), \tag{5}$$

$$\varepsilon_{true} = \ln(1 + \varepsilon), \tag{6}$$

where σ and ε are the measured engineering stress and strain, respectively, based on the original cross-sectional areas of the coupon specimens. The overall true stress-strain relationship was validated by modeling the coupon tensile test. Hancock [27] demonstrated that the yield and tensile strengths of the bent part of the member increased by 22% and 17%, respectively, whereas the elongation reduced by half, thereby increasing the brittleness, which was applied to the material properties.

4.2. Finite Element Analysis Model Verification. A comparison of the experimental-test strengths and displacements considering local buckling with those determined from the corresponding finite element models is shown in Figure 6 and Table 3. Both the finite element models and specimens demonstrated that the stiffness decreased after local buckling owing to common bending, as shown in Figure 7, whereas the strength increased. From the analysis, the strengths V_{LB}, when local buckling occurs in the ISW-320-1.6, ISW-480-1.6, and ISW-640-1.6 analysis models, were 7%, 10%, and 6% higher than those of the specimens, respectively. Considering that boundary conditions, such as screw joints, bolt joints, and jigs, were simplified, the analysis results closely matched the experimental results until the local buckling occurred.

4.3. Parametric Studies. An additional analysis was performed to predict the strength of the integrated members with various specifications. The parameters set in this study are as follows: the steel type, width of the integrated member, and thickness of the integrated member. A general-purpose steel type was selected with reference to KS D 3030. The width of the integrated member was set as 320 mm, 480 mm, and 640 mm as in the test specimens, and the thickness of the integral member was set at intervals of 0.2 mm from a minimum of 0.8 mm to a maximum of 1.8 mm based on the members used in light-gauge steel frames. Table 4 summarizes the analysis results when local buckling occurs in the analysis model with the three parameters.

Figure 8(a) illustrates the relationship between the shear strength at local buckling relative to the nominal flexural strength ($V_{LB}/(M_y/h_1)$) and the width-to-thickness ratio. Figure 8(b) illustrates the relationship between the shear strength at local buckling relative to the nominal flexural strength ($V_{LB}/(M_y/h_1)$) and the slenderness ratio for local buckling ($\lambda_l = \sqrt{M_y/M_{crl,web}}$). The slenderness factor of local buckling (λ_l) includes not only the width-to-thickness ratio of the web element but also the variables of the member yield strength. In Figure 8(a), it can be observed that $V_{LB}/(M_y/h_1)$ decreases when the yield strength (f_y) of the member increases, and the width-to-thickness ratio of the web is the same because the slender ratio of the web element increases. Figure 8(b) confirms that the relationship between the slender ratio (λ_l) for local buckling and strength (V_{LB}) at the occurrence of local buckling can be defined as the nominal flexural strength at yield (M_y).

5. Design Equation of the Cold-Formed Steel-Integrated Member

To apply the nominal shear strength design equation of the integrated member proposed in this study, the following restrictions must be satisfied:

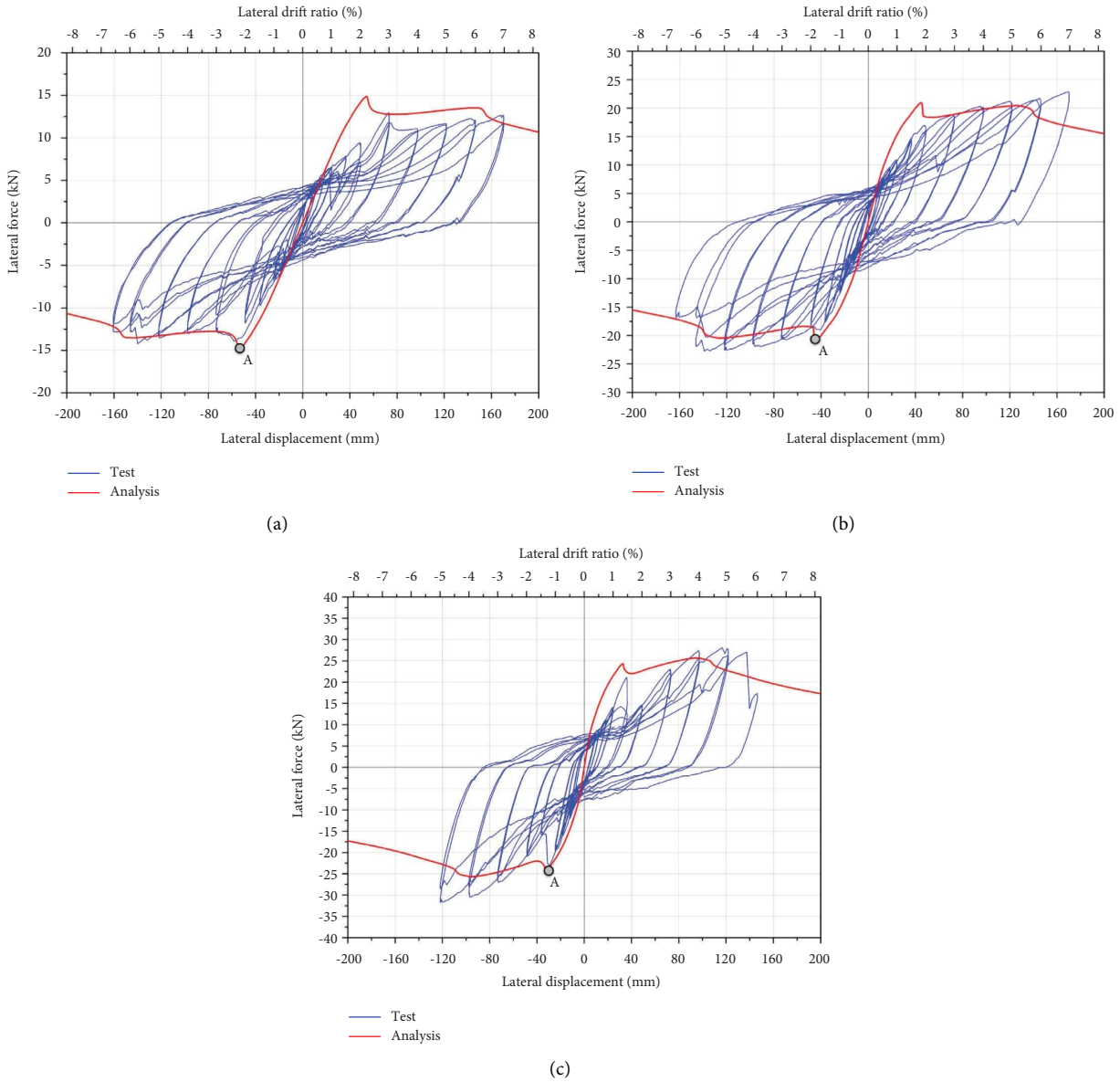

Figure 6: Lateral load-drift ratio relationships of specimens and analysis models (point A: local buckling occurred). (a) ISW-320-1.6; (b) ISW-480-1.6; (c) ISW-640-1.6.

Table 3: Comparison of strength and displacement when local buckling occurs between the specimen and analysis model.

Specimens	Test results*		Analysis results		Comparison	
	$\Delta_{LB,test}$ (mm (%))	$V_{LB,test}$ (kN)	$\Delta_{LB,FEM}$ (mm (%))	$V_{LB,FEM}$ (kN)	$\Delta_{LB,FEM}/\Delta_{LB,test}$	$V_{LB,FEM}/V_{LB,test}$
ISW-320-1.6	58.4 (2.39)	13.9	53.8 (2.20)	14.9	0.92	1.07
ISW-480-1.6	40.5 (1.66)	19.0	44.9 (1.83)	20.9	1.11	1.10
ISW-640-1.6	30.0 (1.23)	23.0	32.9 (1.34)	24.4	1.10	1.06

*Test results for negative direction with no out-of-plane displacement.

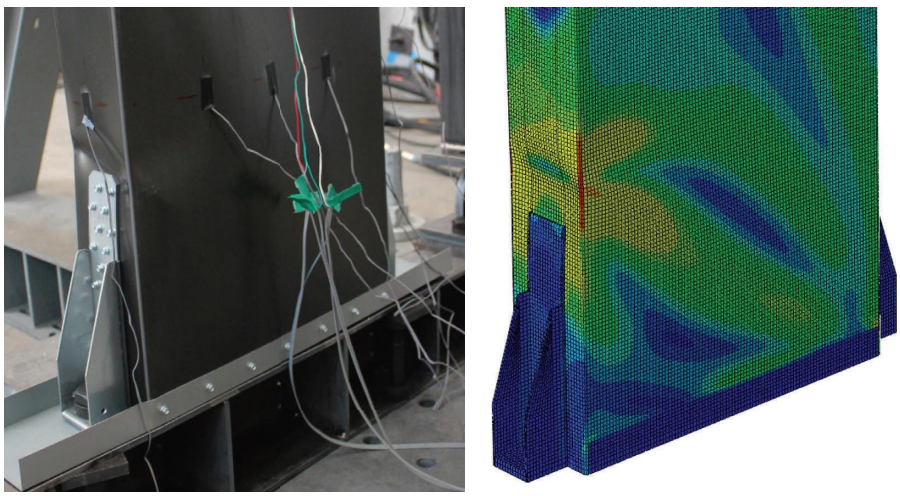

(a) (b)

Figure 7: The failure mode of the ISW-480-1.6 specimen and analysis model. (a) Specimen; (b) analysis model.

Table 4: Analysis models of strengths when local buckling occurs.

Steel types	Web width-to-thickness ratio	$V_{LB,FEM}$ (kN)			
		SGMC245Y	SGMC295Y	SGMC335Y	SGMC365Y
ISW-320-0.8	394	3.7	4.4	4.6	4.8
ISW-320-1.0	314	5.4	6.0	6.4	6.7
ISW-320-1.2	261	7.7	8.3	9.4	10.0
ISW-320-1.4	223	9.6	10.6	11.6	12.2
ISW-320-1.6	194	11.8	13.5	14.6	15.4
ISW-320-1.8	172	14.3	16.4	17.9	18.6
ISW-480-0.8	594	4.9	5.4	5.8	6.0
ISW-480-1.0	474	7.1	7.9	8.5	8.7
ISW-480-1.2	394	10.4	11.3	11.9	12.4
ISW-480-1.4	337	12.8	15.0	15.8	16.9
ISW-480-1.6	294	17.4	19.3	20.7	21.9
ISW-480-1.8	261	21.2	24.0	25.8	26.9
ISW-640-0.8	794	5.2	6.0	6.4	6.4
ISW-640-1.0	634	8.7	9.6	10.2	10.7
ISW-640-1.2	527	12.1	13.2	13.7	14.6
ISW-640-1.4	451	16.6	18.2	19.4	20.4
ISW-640-1.6	394	21.3	23.4	25.0	26.1
ISW-640-1.8	350	26.7	29.3	31.2	32.6

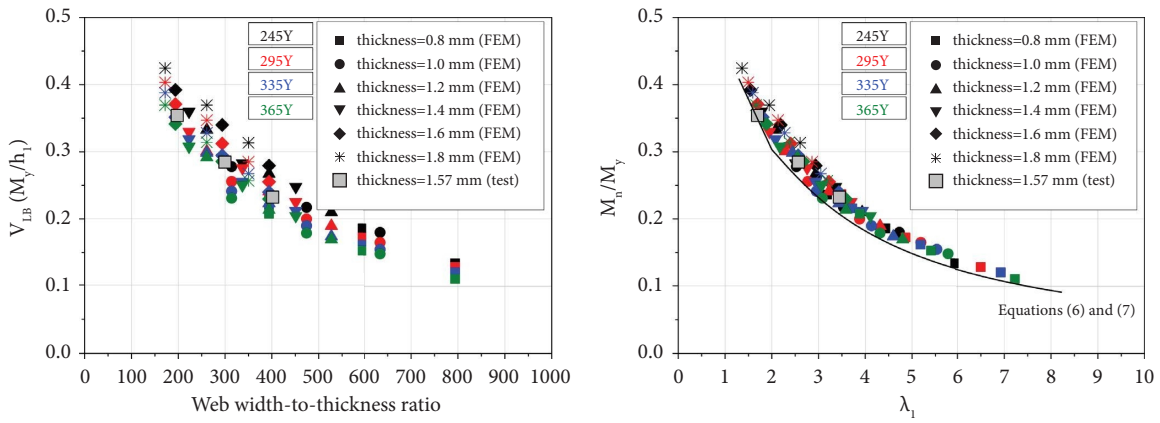

(a) (b)

Figure 8: Relationship between the shear strength at local buckling relative to the nominal flexural strength and web slenderness. (a) Web width-to-thickness ratio; (b) slenderness factor.

(1) The height of the cross section must be 320 mm or more and 640 mm or less.

(2) The thickness of the cross section must be 0.8 mm or more and 1.8 mm or less.

(3) The yield strength of steels constituting must be 245 MPa or more and 365 MPa or less.

The nominal flexural strength of the CFS-integrated member based on 72 analysis models and three specimens is as follows:

$$\text{For } \lambda_{l,\text{web}} \le 2.0, \quad M_{n,\text{ISW}} = \left(0.603 - 0.15\sqrt{\frac{F_y}{F_{\text{crl,web}}}}\right) M_y, \tag{7}$$

$$\text{For } \lambda_{l,\text{web}} > 2.0, \quad M_{n,\text{ISW}} = \left[1 - 0.75\left(\frac{F_y}{F_{\text{crl,web}}}\right)^{0.55}\right]\left(\frac{F_y}{F_{\text{crl,web}}}\right)^{0.55} M_y, \tag{8}$$

where $\lambda_{l,\text{web}}$ is the slenderness factor of the local buckling for the integrated member, $F_{\text{crl,web}} (= k(\pi^2 E/12(1-\mu^2))(t/w)^2)$ is the local buckling stress of the integrated member according to AISI S100-16 [15], $M_y (= S_f F_y)$ is the member yield moment, and S_f is the elastic section modulus.

In general, the finite element analysis results show higher strength than the experimental results; hence, as shown in Figure 8(b), the analysis results are placed at the upper end of equations (6) and (7). The $V_{\text{LB,FEM}}/(M_y/h_1)$ value had an average value of 1.092 for the 72 analysis models. Considering that the strengths during local buckling of the ISW-320-1.6, ISW-480-1.6, and ISW-640-1.6 analysis models were respectively 7%, 10%, and 6% higher than when local buckling of the specimen occurs, the nominal flexural strength of the integrated member accurately evaluates the nominal flexural strength of the specimen.

The nominal shear strength of the CFS-integrated member is as follows:

$$V_{n,\text{ISW}} = \frac{M_{n,\text{ISW}}}{h_1}. \tag{9}$$

6. Design Example

In this section, a design example of a C-$500 \times 100 \times 40 \times 1.5$ mm-integrated member is presented. The inner radius of the integrated member was twice its thickness. The nominal yield stresses of both the framing and sheathing were 270 MPa. The heights of the integrated member and hold-down were 2,500 mm and 500 mm, respectively. This design example assumes that the actual material properties are obtained from the coupon tests, and the actual material properties are used in the calculation. The nominal shear strength was determined using the following steps:

The slenderness factor

$$\begin{aligned}\lambda_{l,\text{web}} &= \sqrt{\frac{M_y}{M_{\text{crl,web}}}} = \sqrt{\frac{F_y}{F_{\text{crl,web}}}} = \sqrt{\frac{F_y}{k\left(\pi^2 E/12\left(1-\mu^2\right)\right)(t/w)^2}} \\ &= \sqrt{\frac{270}{24\left(\pi^2 \times 203,000/12\left(1-0.3^2\right)\right)(1.5/500 - 1.5\times 6)^2}} = \sqrt{\frac{270}{41.10}} = 2.56 > 2.0.\end{aligned} \tag{10}$$

The nominal flexural strength

$$\begin{aligned}\text{For } \lambda_{l,\text{web}} > 2.0, M_{n,\text{ISW}} &= \left[1 - 0.75\left(\frac{F_y}{F_{\text{crl,web}}}\right)^{0.55}\right]\left(\frac{F_y}{F_{\text{crl,web}}}\right)^{0.55} M_y \\ &= \left[1 - 0.75\left(\frac{F_y}{F_{\text{crl,web}}}\right)^{0.55}\right]\left(\frac{F_y}{F_{\text{crl,web}}}\right)^{0.55} S_f F_y \\ &= \left[1 - 0.75\left(\frac{270}{41.10}\right)^{0.55}\right]\left(\frac{270}{41.10}\right)^{0.55}\left(159,510 \times 270 \times 10^{-6}\right) \\ &= 11.23\text{kN}\bullet m.\end{aligned} \tag{11}$$

The nominal shear strength

$$V_{n,\mathrm{ISW}} = \frac{M_{n,\mathrm{ISW}}}{h_1} = \frac{(11.23\mathrm{kN}\bullet m)}{(2.5m - 0.5m \times 2)/2} = 15.0\,\mathrm{kN}. \quad (12)$$

7. Conclusion

In this study, we proposed a design equation that takes into account the changes in web width-to-thickness ratio for the integrated member, which can serve as an alternative to steel sheet in light-gauge steel frames. The proposed design equation for cold-formed steel integrated shear walls was validated by three specimens and 72 finite element models and showed good agreement with the results, enabling designers to determine the strength of these shear walls without conducting full-scale shear wall tests. In the cross-section of the integrated shear wall defined in this paper, the load-displacement relationship was dominated by local buckling due to bending. Therefore, even if the cross-sectional width of the integrated member exceeds 640 mm and the web width-to-thickness ratio of the integrated member is 800 or less, the design formula proposed in this study can be applied, but verification is required.

Data Availability

The experimental data and analysis data used to support the findings of this study are available from the corresponding author upon request.

Conflicts of Interest

The authors declare that they have no conflicts of interest.

Acknowledgments

This research was supported by the Basic Science Research Program through the National Research Foundation of Korea (NRF) funded by the Ministry of Education (grant no. 2021R1A6A3A01087798).

References

[1] S. A. Chini and K. Gupta, "A comparison between steel and wood residential framing systems," *The Nation*, vol. 700, no. 12, pp. 4–880, 1997.

[2] Y. Yong, C. Yunpeng, D. Yongjun, X. Bin, and G. Xiaoyan, "Numerical simulation of the cold-formed thin-walled steel structure system," *Build. Struct.*vol. 2, pp. 41–45, 2011.

[3] W. Yang and Q. Yang, "Study on the dynamic characteristics of light steel residential structural system," *Engineering*, vol. 09, no. 06, pp. 591–598, 2017.

[4] D. Y. Lee, B. H. Cho, D. I. Jung, J. S. Lee, and K. W. Lee, "Experimental study on the cyclic behavior of integrated panels for cold-formed steel shear wall system," *Applied Sciences*, vol. 10, no. 5, p. 1649, 2020.

[5] R. Serrette, "Behavior of cyclically loaded light gauge steel framed shear walls," in *Building to Last,*American Society of Civil Engineers, Reston, VA, USA, 1997.

[6] N. Yanagi and C. Yu, "Effective strip method for the design of cold-formed steel framed shear wall with steel sheet sheathing," *Journal of Structural Engineering*, vol. 140, no. 4, Article ID 04013101, 2014.

[7] C. Yu, "Shear resistance of cold-formed steel framed shear walls with 0.686 mm, 0.762 mm, and 0.838 mm steel sheet sheathing," *Engineering Structures*, vol. 32, no. 6, pp. 1522–1529, 2010.

[8] C. Yu and Y. Chen, "Detailing recommendations for 1.83 m wide cold-formed steel shear walls with steel sheathing," *Journal of Constructional Steel Research*, vol. 67, no. 1, pp. 93–101, 2011.

[9] X. Wang, E. Pantoli, T. C. Hutchinson et al., "Seismic performance of cold-formed steel wall systems in a full-scale building," *Journal of Structural Engineering*, vol. 141, no. 10, Article ID 04015014, 2015.

[10] S. G. Hong, B. H. Cho, K. S. Chung, and J. H. Moon, "Behavior of framed modular building system with double skin steel panels," *Journal of Constructional Steel Research*, vol. 67, no. 6, pp. 936–946, 2011.

[11] L. Fiorino, V. Macillo, and R. Landolfo, "Experimental characterization of quick mechanical connecting systems for cold-formed steel structures," *Advances in Structural Engineering*, vol. 20, no. 7, pp. 1098–1110, 2017.

[12] A. Zhang, Z. Xie, W. Yan, Y. Zhang, and D. Zhou, "Experimental investigation of CFS steel sheathed shear walls with openings using self-piercing rivets," *Thin-Walled Structures*, vol. 138, pp. 313–325, 2019.

[13] W. Zhang, M. Mahdavian, X. Lan, and C. Yu, "Cold-formed steel framed shear walls with in-frame corrugated steel sheathing," *Journal of Structural Engineering*, vol. 147, no. 12, Article ID 04021210, 2021.

[14] M. Rahimibala, F. R. Rofooei, F. Farahbod, and O. Pourabdollah, "Experimental-numerical assessment of laterally-loaded CFS frames with steel sheathing and K-shaped braces," *Journal of Constructional Steel Research*, vol. 203, Article ID 107792, 2023.

[15] American Iron and Steel Institute (Aisi), *North American Specifications for the Design of Cold-Formed Steel Structural Members*, American Iron and Steel Institute, Washington, DC, USA, 2016.

[16] J. DaBreo and C. A. Rogers, *Steel Sheathed Shear walls Subjected to Combined Lateral and Gravity Loads*, Department of Civil Engineering and Applied Mechanics, McGill University, Montreal, Canada, 2012.

[17] C. Ong-Tone, *Tests and Evaluation of Cold-Formed Steel Frame*, Department of Civil Engineering and Applied Mechanics, McGill University, Montreal, Australia, 2009.

[18] C. A. Rogers, N. Balh, C. Ong-Tone, I. Shamim, and J. DaBreo, "Development of seismic design provisions for steel sheet sheathed shear walls," in *Proceedings of the Structures Congress 2011*, pp. 676–687, Las Vegas, NA, USA, April 2011.

[19] H. Moghimi and H. R. Ronagh, "Performance of light-gauge cold-formed steel strap-braced stud walls subjected to cyclic loading," *Engineering Structures*, vol. 31, no. 1, pp. 69–83, 2009.

[20] M. Zeynalian and H. R. Ronagh, "An experimental investigation on the lateral behavior of knee-braced cold-formed steel shear walls," *Thin-Walled Structures*, vol. 51, pp. 64–75, 2012.

[21] A. Mirzaei, R. H. Sangree, K. Velchev et al., "Seismic capacity-based design of narrow strap-braced cold-formed steel walls," *Journal of Constructional Steel Research*, vol. 115, pp. 81–91, 2015.

[22] P. Clark, K. Frank, H. Krawinkler, and R. Shaw, "Protocol for fabrication, inspection, testing, and documentation of beam-

column connection tests and other experimental specimens," SAC Steel Project Background Document, California, VA, USA, SAC/BD-97/02, 1997.

[23] American Society for Testing and Materials (Astm), *Standard Test Methods for Cyclic (Reversed) Load Test for Shear Resistance of Vertical Elements of the Lateral Force Resisting Systems for Buildings*, American National Standards Institute, Washington, DC, USA, 2009.

[24] S. E. Kim and D. H. Lee, "Second-order distributed plasticity analysis of space steel frames," *Engineering Structures*, vol. 24, no. 6, pp. 735–744, 2002.

[25] A. Susila and J. Tan, "Flexural strength performance and buckling mode prediction of cold-formed steel (C section)," *Procedia Engineering*, vol. 125, pp. 979–986, 2015.

[26] H. D. Craveiro, R. Rahnavard, L. Laím, R. A. Simões, and A. Santiago, "Buckling behavior of closed built-up cold-formed steel columns under compression," *Thin-Walled Structures*, vol. 179, Article ID 109493, 2022.

[27] G. J. Hancock, "Cold-formed steel structures," *Journal of Constructional Steel Research*, vol. 59, no. 4, pp. 473–487, 2003.